Download is permitted to HPC-Lab members and for educational purposes only

Discrete Element Modelling of the Failure of Anisotropic Laminated Composite Shells

S. Mohammadi

Department of Civil Engineering, University of Wales Swansea
Singleton Park, Swansea SA2 8PP, U.K.

Abstract

An innovative approach is presented for fracture analysis of composites subjected to impact loading. This approach is based on discontinuum concepts of the combined finite/discrete element algorithm for damage analysis of progressive fractured media. An anisotropic softening Hoffman failure criterion is implemented for determining the initiation and propagation of a crack. Integration of the flow rule is performed by the backward Euler method combined with a Newton-Raphson iteration scheme. The algorithm comprises various contact detection and contact interaction schemes to construct an efficient and reliable tool for the modelling of complex post failure phenomena. A set of numerical tests is provided to assess the performance of the algorithm.

1 Introduction

Gradually replacing conventional materials, composite laminates are now widely used in many applications involving dynamic loading such as machinery, pressure vessels, defense structures, vehicles, sport equipment and notably aerospace structures [1]. Industries such as the automotive, and recreational industries have also been placing increased reliance on for high performance composite materials.

One of the major problems that affects the design and performance of composite materials for structural applications is their vulnerability to transverse impact which may cause substantial internal damage of the component due to matrix cracking, fibre failure and delamination [2]. In general, according to the orthotropic laminated nature of composites, the failure modes may be classified into four different types : matrix failure, delamination, shear cracking, and erosion damage. There is, however, agreement that the most dominant causes of damage during impact are matrix cracking coupled strongly with complex mode delamination mechanisms. These failure modes are accompanied by steep stress gradients and are usually encountered in regions such as free edges, ply termination, zone of delamination, and voids and holes.

Recent developments of discrete element methods (DEM) have opened a new approach to modelling this behaviour based on discontinuum mechanics. In this study, a combined finite/discrete element algorithm is developed to predict initiation, propagation and interaction of fracture and delamination phenomena in composites. This algorithm could be used for the analysis of reinforced concrete and masonry structures, for which a progressive fragmentation process is predictable under the impact and explosive loadings.

2 Discrete Element Modelling

Consider a composite specimen subjected to an impact loading as depicted in Figure 1a. Early material cracks and interlaminar debondings are likely to appear near the position

of applied impact load. In a combined FE/DE method, the possibly fractured region is modelled using a discrete element mesh and the remainder of the specimen is modelled by a standard finite element mesh. It is also possible to model the whole structure with discrete elements; in which case the possibility of cracking is investigated throughout the structure. A combined mesh enables us to prevent unnecessary contact detection and interaction calculations which comprise a major part of the analysis time [3].

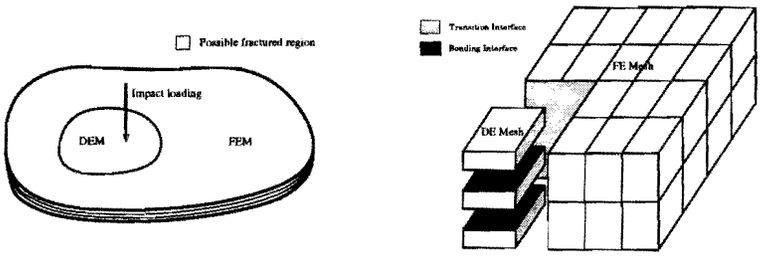

Figure 1: Discrete element modelling of a composite plate.

Each ply or a group of similar plies is modelled by one discrete element (Figure 1b). Each discrete element will be discretized by a finite element mesh and may have nonlinear material properties or geometric nonlinearities (large deformations). The interlaminar behaviour of discrete elements is governed by bonding laws, including contact and friction interactions for the post delamination phase. Interactions between finite elements (not those which are used for DEM discretization) and discrete elements are modelled by transition interfaces. A transition interface is defined as a normal interface with very high bonding strengths which prevent debonding under all loading conditions. All interfaces, are firstly monitored against the delamination criterion. Once two layers are delaminated, the corresponding interface will still be capable of further contact and friction interaction. However, there will be no re-bonding after delamination.

One important aspect of this type of modelling, which distinguishes it from other contact based delamination algorithms [4], is that it does not require any predefined interface element. Being free from the restrictions of interface elements provides major advantages: Firstly, there is no need for the nodes on different layers to match each other, which eases the way in which data is prepared. This is essential in defining the transition interfaces. Secondly, in progressive cracking, we may end up with new nodes, edges and boundaries that could destroy the compatibility required for these interface elements. Further discussions about this method are out of scope of this paper and the reader is referred to [5].

3 Anisotropic Strength Criteria

Most available strength information is based on an uniaxial stress state, while practical applications invariably involve at least biaxial loading. Unlike isotropic materials, the strength of composites is typically directionally dependent. Furthermore, failure of some plies of a laminated structure need not necessarily constitute rupture of the total laminate since multiple layers may provide other sustaining load paths [6].

Several of the anisotropic strength or failure theories are extensions of isotropic yield criteria. Hill (1950) generalized von Mises' formulation to include anisotropy. A variation of maximum stress theory for unidirectional composites was proposed by Stowell and Liu [7] in which the failure stress of the fibres was taken as the limiting strength of the lamina in the fibre direction, while the limiting transverse and shear stresses are those of the matrix. Hoffman [8], in 1967, altered Hill's criterion to provide for unequal tensile and compressive strengths by introducing linear terms in the functional form. Attempts to develop a strength theory which is invariant with respect to the coordinate system were led to the development of the Tsai-Wu criterion in 1971 [9]. Lack of accurate multiaxial material parameters usually

leads to use of simplified version of this criterion, i.e. the Hoffman criterion.

3.1 Hoffman Anisotropic Yield Criterion

According to the Hoffman criterion, a geometrical yield surface is constructed from three tensile yield strengths $\bar{\sigma}_{iiT}$, three compressive yield strengths $\bar{\sigma}_{iiC}$, and three shear yield strengths $\bar{\sigma}_{ij}, i \neq j$. It may be defined as :

$$\Phi = \frac{1}{2}\boldsymbol{\sigma}^T \boldsymbol{P} \boldsymbol{\sigma} + \boldsymbol{\sigma}^T \boldsymbol{p} - \bar{\sigma}^2(\kappa) \tag{1}$$

where the projection matrix $\boldsymbol{P}$, and the projection vector $\boldsymbol{p}$ are defined based on the nine material yield strengths and a normalised yield strength $\bar{\sigma}$,

$$\boldsymbol{\sigma} = \begin{pmatrix} \sigma_{11} & \sigma_{22} & \sigma_{33} & \sigma_{12} & \sigma_{23} & \sigma_{31} \end{pmatrix}^T \tag{2}$$

$$\boldsymbol{P} = \begin{bmatrix} 2(\alpha_{31}+\alpha_{12}) & -2\alpha_{12} & -2\alpha_{31} & 0 & 0 & 0 \\ -2\alpha_{12} & 2(\alpha_{23}+\alpha_{12}) & -2\alpha_{23} & 0 & 0 & 0 \\ -2\alpha_{31} & -2\alpha_{23} & 2(\alpha_{31}+\alpha_{23}) & 0 & 0 & 0 \\ 0 & 0 & 0 & 6\alpha_{44} & 0 & 0 \\ 0 & 0 & 0 & 0 & 6\alpha_{55} & 0 \\ 0 & 0 & 0 & 0 & 0 & 6\alpha_{66} \end{bmatrix} \tag{3}$$

$$\boldsymbol{p}^T = \begin{bmatrix} \alpha_{11} & \alpha_{22} & \alpha_{33} & 0 & 0 & 0 \end{bmatrix} \tag{4}$$

where

$$\begin{aligned}
\alpha_{11} &= \bar{\sigma}^2 \left(\frac{\bar{\sigma}_{11C} - \bar{\sigma}_{11T}}{\bar{\sigma}_{11C}\bar{\sigma}_{11T}} \right) \quad , \quad \alpha_{44} = \frac{\bar{\sigma}^2}{3\bar{\sigma}_{23}^2} \\
\alpha_{22} &= \bar{\sigma}^2 \left(\frac{\bar{\sigma}_{22C} - \bar{\sigma}_{22T}}{\bar{\sigma}_{22C}\bar{\sigma}_{22T}} \right) \quad , \quad \alpha_{55} = \frac{\bar{\sigma}^2}{3\bar{\sigma}_{31}^2} \\
\alpha_{33} &= \bar{\sigma}^2 \left(\frac{\bar{\sigma}_{33C} - \bar{\sigma}_{33T}}{\bar{\sigma}_{33C}\bar{\sigma}_{33T}} \right) \quad , \quad \alpha_{66} = \frac{\bar{\sigma}^2}{3\bar{\sigma}_{12}^2} \\
\alpha_{12} &= \frac{\bar{\sigma}^2}{2} \left(\frac{1}{\bar{\sigma}_{11T}\bar{\sigma}_{11C}} + \frac{1}{\bar{\sigma}_{22T}\bar{\sigma}_{22C}} - \frac{1}{\bar{\sigma}_{33T}\bar{\sigma}_{33C}} \right) \\
\alpha_{23} &= \frac{\bar{\sigma}^2}{2} \left(\frac{1}{\bar{\sigma}_{22T}\bar{\sigma}_{22C}} + \frac{1}{\bar{\sigma}_{33T}\bar{\sigma}_{33C}} - \frac{1}{\bar{\sigma}_{11T}\bar{\sigma}_{11C}} \right) \\
\alpha_{31} &= \frac{\bar{\sigma}^2}{2} \left(\frac{1}{\bar{\sigma}_{33T}\bar{\sigma}_{33C}} + \frac{1}{\bar{\sigma}_{11T}\bar{\sigma}_{11C}} - \frac{1}{\bar{\sigma}_{22T}\bar{\sigma}_{22C}} \right)
\end{aligned} \tag{5}$$

3.1.1 Integration of the Rate Equation

The key issue of computational plasticity models is often the integration of the flow rule in a finite time step. For this purpose, the backward Euler method coupled with the Newton-Raphson iterative scheme is used; which has been found to be generally stable and efficient [10]. For the j^{th} load step, the additivity postulate is used for strain decomposition,

$$\Delta\boldsymbol{\epsilon}_j = \Delta\boldsymbol{\epsilon}_j^{el} + \Delta\boldsymbol{\epsilon}_j^{pl} \tag{6}$$

Applying the linear elastic stress-strain relationship and the associated flow rule,

$$\Delta\boldsymbol{\epsilon}_j = \boldsymbol{C}\Delta\boldsymbol{\sigma}_j + \Delta\lambda_j \frac{\partial\Phi}{\partial\boldsymbol{\sigma}_j} \tag{7}$$

where $\Delta\lambda_j$ is the plastic multiplier. The derivative of Φ (1) with respect to $\boldsymbol{\sigma}_j$ is the flow vector $\boldsymbol{a}$,

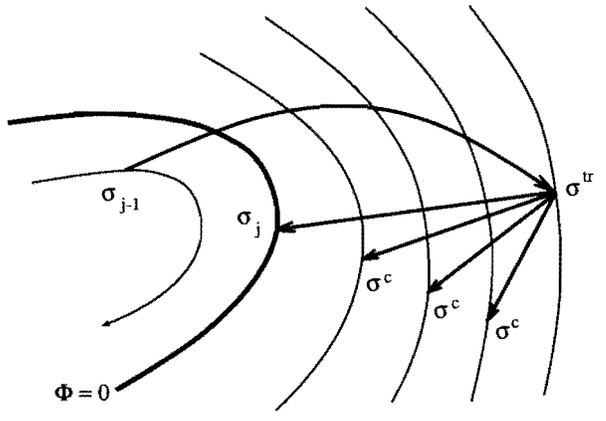

Figure 2: Stress return algorithm based on the Euler backward method.

$$\boldsymbol{a} = \frac{\partial \Phi}{\partial \boldsymbol{\sigma}_j} = \boldsymbol{P}_\alpha \boldsymbol{\sigma}_j + \boldsymbol{p}_\alpha \tag{8}$$

Rewriting equation (7) with the aid of $\boldsymbol{C}\boldsymbol{\sigma}_{j-1} - \boldsymbol{\epsilon}^{el}_{j-1} = \boldsymbol{0}$, will eventually result in

$$(\boldsymbol{C} + \Delta\lambda_j \boldsymbol{P}_\alpha)(\boldsymbol{\sigma}_{i-1} + \Delta\boldsymbol{\sigma}_j) - (\boldsymbol{\epsilon}^{el}_{i-1} + \Delta\boldsymbol{\epsilon}_j - \Delta\lambda_j \boldsymbol{p}_\alpha) = 0 \tag{9}$$

Then, the final stress at the end of the iteration is solved from this relation (Figure 2)

$$\boldsymbol{\sigma}_j = \boldsymbol{\sigma}_{i-1} + \Delta\boldsymbol{\sigma}_j \tag{10}$$

$$\boldsymbol{\sigma}_j = (\boldsymbol{C} + \Delta\lambda_j \boldsymbol{P}_\alpha)^{-1} (\boldsymbol{\epsilon}^{el}_{i-1} + \Delta\boldsymbol{\epsilon}_j - \Delta\lambda_j \boldsymbol{p}_\alpha) \tag{11}$$

which can be rewritten in terms of the $\boldsymbol{D}$ matrix

$$\boldsymbol{\sigma}_j = \boldsymbol{D}(\boldsymbol{I} + \Delta\lambda_j \boldsymbol{D}\boldsymbol{P}_\alpha)^{-1} (\boldsymbol{\epsilon}^{el}_{i-1} + \Delta\boldsymbol{\epsilon}_j - \Delta\lambda_j \boldsymbol{p}_\alpha) \tag{12}$$

Linearization of Φ with respect to $\Delta\lambda$ gives,

$$\Delta\lambda_j^{k+1} = \Delta\lambda_j^k - \left. \frac{\Phi(\Delta\lambda_j)}{\frac{\partial \Phi}{\partial \Delta\lambda_j}} \right|_{\Delta\lambda_j^k} \tag{13}$$

Hence, the derivative of Φ with respect to $\Delta\lambda_j$ is now needed. For hardening or softening materials, Φ is also a function of the hardening/softening parameter, κ. Therefore,

$$\frac{\partial \Phi}{\partial \Delta\lambda_j} = \left(\frac{\partial \Phi}{\partial \boldsymbol{\sigma}_j}\right)^T \frac{\partial \boldsymbol{\sigma}_j}{\partial \Delta\lambda_j} + \frac{\partial \Phi}{\partial \bar{\sigma}} \frac{\partial \bar{\sigma}}{\partial \kappa} \frac{\partial \kappa}{\partial \Delta\lambda_j} \tag{14}$$

The first part of the first term is the flow vector $\boldsymbol{a}$, and (12) is used for the second part

$$\frac{\partial \boldsymbol{\sigma}_j}{\partial \Delta\lambda_j} = -\boldsymbol{D}(\boldsymbol{I} + \Delta\lambda_j \boldsymbol{D}\boldsymbol{P}_\alpha)^{-1} \left[\boldsymbol{D}(\boldsymbol{I} + \Delta\lambda_j \boldsymbol{D}\boldsymbol{P}_\alpha)^{-1} \boldsymbol{P}_\alpha (\boldsymbol{\epsilon}^{el}_{i-1} + \Delta\boldsymbol{\epsilon}_j - \Delta\lambda_j \boldsymbol{p}_\alpha) + \boldsymbol{p}_\alpha\right] \tag{15}$$

To evaluate the second term, an isotropic strain hardening law is adopted [11]

$$\Delta\epsilon^p_{eff} = \sqrt{\frac{2}{3}} \Delta\lambda_j \sqrt{\Delta\boldsymbol{\epsilon}^p \Delta\boldsymbol{\epsilon}^p} \tag{16}$$

$$\kappa = \sqrt{\frac{2}{3}}\Delta\lambda_j \left(\boldsymbol{a}^T\boldsymbol{a}\right)^{\frac{1}{2}} \tag{17}$$

and from equation (1)

$$\frac{\partial\Phi}{\partial\bar{\sigma}} = -2\bar{\sigma} \tag{18}$$

$$\frac{\partial\bar{\sigma}}{\partial\kappa} = H \tag{19}$$

$$\frac{\partial\kappa}{\partial\Delta\lambda_j} = \sqrt{\frac{2}{3}}\left[A + \frac{\Delta\lambda_j}{A}\boldsymbol{a}\boldsymbol{P}_\alpha\frac{\partial\boldsymbol{\sigma}_j}{\partial\Delta\lambda_j}\right] \tag{20}$$

Therefore, from (14), one gets

$$\frac{\partial\Phi}{\partial\Delta\lambda_j} = \boldsymbol{a}^T\frac{\partial\boldsymbol{\sigma}_j}{\partial\Delta\lambda_j} - 2\sqrt{\frac{2}{3}}\bar{\sigma}H\left[A + \frac{\Delta\lambda_j}{A}\boldsymbol{a}\boldsymbol{P}_\alpha\frac{\partial\boldsymbol{\sigma}_j}{\partial\Delta\lambda_j}\right] \tag{21}$$

where $A = \left(\boldsymbol{a}^T\boldsymbol{a}\right)^{\frac{1}{2}}$ and H is the hardening/softening slope. Box 1 summarizes the stress return algorithm for the Hoffman yield surface with isotropic hardening/softening.

3.1.2 Consistent Tangent Matrix

To evaluate the consistent tangent matrix, the total strain at the end of load step j may be expressed as,

$$\boldsymbol{\epsilon}_j = \boldsymbol{\epsilon}_{j-1} + \Delta\boldsymbol{\epsilon}_j^{el} + \Delta\boldsymbol{\epsilon}_j^{pl} \tag{22}$$

With the relations for incremental elastic and plastic strains, the stress-strain relationship can be written as

$$\boldsymbol{\epsilon}_j = \boldsymbol{\epsilon}_{j-1} + \boldsymbol{C}\left(\boldsymbol{\sigma}_j - \boldsymbol{\sigma}_{j-1}\right) + \Delta\lambda_j\frac{\partial\Phi}{\partial\boldsymbol{\sigma}_j} \tag{23}$$

Taking the time derivative of (23) results in

$$\dot{\boldsymbol{\epsilon}}_j = \boldsymbol{C}\dot{\boldsymbol{\sigma}}_j + \Delta\lambda_j\frac{\partial^2\Phi}{\partial\boldsymbol{\sigma}_j^2}\dot{\boldsymbol{\sigma}}_j + \dot{\lambda}_j\frac{\partial\Phi}{\partial\boldsymbol{\sigma}_j} \tag{24}$$

or in terms of the $\boldsymbol{D}$ matrix,

$$\dot{\boldsymbol{\sigma}}_j = \boldsymbol{D}\dot{\boldsymbol{\epsilon}}_j - \dot{\lambda}_j\boldsymbol{D}\frac{\partial\Phi}{\partial\boldsymbol{\sigma}_j} - \Delta\lambda_j\boldsymbol{D}\frac{\partial^2\Phi}{\partial\boldsymbol{\sigma}_j^2}\dot{\boldsymbol{\sigma}}_j \tag{25}$$

The last term in (25) vanishes for infinitesimal increments, which results in the classical elastoplastic tangent stiffness matrix. For finite loading increments, however, the contribution of this term becomes significant. Re-arranging (25) with the aid of $\frac{\partial\Phi}{\partial\boldsymbol{\sigma}_j} = \boldsymbol{a}$ and $\frac{\partial^2\Phi}{\partial\boldsymbol{\sigma}_j^2} = \boldsymbol{P}_\alpha$, results in

$$\dot{\boldsymbol{\sigma}}_j = \boldsymbol{Q}\left(\dot{\boldsymbol{\epsilon}}_j - \dot{\lambda}_j\boldsymbol{a}\right) \tag{26}$$

$$\boldsymbol{Q} = \boldsymbol{D}\left(\boldsymbol{I} + \Delta\lambda_j\boldsymbol{D}\boldsymbol{P}_\alpha\right)^{-1} \tag{27}$$

To evaluate $\dot{\lambda}$, the consistency condition is considered

$$\dot{\Phi} = \boldsymbol{a}^T\dot{\boldsymbol{\sigma}}_j + B\dot{\lambda}_j = 0 \tag{28}$$

where B is the second term in (14),

Box 1. Stress return algorithm for Hoffman yield surface.

- Compute trial stress (Elastic prediction phase)

  $\boldsymbol{\sigma}^{tr} = \boldsymbol{\sigma}_{j-1} + \boldsymbol{D}\Delta\boldsymbol{\epsilon}$

- Compute yield function for $\boldsymbol{\sigma}^{tr}$

  $\Phi^{tr} = \sigma^{tr}_{eff} - \bar{\sigma}^2$ (1)

- IF $\Phi^{tr} \leq 0$ (Elastic update)

  $\boldsymbol{\sigma}_j = \boldsymbol{\sigma}^{tr}$

- ELSE (Elastoplastic update)

  Iterative loop for Plastic correction phase

  Compute stress at point of return (c)

  $\boldsymbol{\sigma}^c = [\boldsymbol{I} + \Delta\boldsymbol{D}\boldsymbol{P}_\alpha]^{-1}[\boldsymbol{\sigma}^{tr} - \Delta\lambda\boldsymbol{D}\boldsymbol{P}_\alpha]$ (12)

  Compute current yield stress and softening modulus

  H , $\bar{\sigma}^c(\kappa) = \bar{\sigma} + \epsilon^{pl}_{eff}H$

  Compute current yield function

  $\Phi^c = \sigma^c_{eff} - (\bar{\sigma}^c)^2$ (1)

  IF $\left|\Phi^c/(\bar{\sigma}^c)^2\right| \leq TOLER$

  $\boldsymbol{\sigma}_j = \boldsymbol{\sigma}^c$

  ELSE

  $\boldsymbol{a} = \frac{\partial\Phi}{\partial\boldsymbol{\sigma}_c} = \boldsymbol{P}_\alpha\boldsymbol{\sigma}_c + \boldsymbol{p}_\alpha$

  $A = (\boldsymbol{a}^T\boldsymbol{a})^{\frac{1}{2}}$, $\epsilon^{pl}_{eff} = \sum\sqrt{\frac{2}{3}}\Delta\lambda A$ (16)

  $\frac{\partial\boldsymbol{\sigma}}{\partial\Delta\lambda}$ from (15)

  $FIRST = \boldsymbol{a}^T\frac{\partial\boldsymbol{\sigma}}{\partial\Delta\lambda}$

  $SECOND = 2\sqrt{\frac{2}{3}}\bar{\sigma}H\left[A + \frac{\Delta\lambda_j}{A}\boldsymbol{a}\boldsymbol{P}_\alpha\frac{\partial\boldsymbol{\sigma}_j}{\partial\Delta\lambda_j}\right]$ (21)

  $\Delta\lambda_j^{k+1} = \Delta\lambda_j^k - \frac{\Phi^c}{FIRST+SECOND}$ (13)

  Next iteration

  ENDIF

- ENDIF

$$B = \frac{\partial\Phi}{\partial\bar{\sigma}}\frac{\partial\bar{\sigma}}{\partial\kappa}\frac{\partial\kappa}{\partial\Delta\lambda_j} \tag{29}$$

By premultiplying (26) by $\boldsymbol{a}^T$ and then substituting into (29), $\dot{\lambda}$ may then be solved for

$$\dot{\lambda}_j = \frac{\boldsymbol{a}^T\boldsymbol{Q}}{B + \boldsymbol{a}^T\boldsymbol{Q}\boldsymbol{a}}\dot{\boldsymbol{\epsilon}}_j \tag{30}$$

and when substituting back into (26) yields,

$$\dot{\boldsymbol{\sigma}}_j = \boldsymbol{D}_{ct}\dot{\boldsymbol{\epsilon}}_j \tag{31}$$

where the consistent tangent matrix, $\boldsymbol{D}_{ct}$, is given by

$$\boldsymbol{D}_{ct} = \boldsymbol{Q}\left[\boldsymbol{I} - \frac{\boldsymbol{a}\boldsymbol{a}^T\boldsymbol{Q}}{B + \boldsymbol{a}^T\boldsymbol{Q}\boldsymbol{a}}\right] \tag{32}$$

4 Crack Propagation

For the material fracture, in concept, normal hardening plasticity procedures can be applied to softening materials by simply introducing a softening rather than a hardening equivalent stress - equivalent plastic strain relationship. In practice, however, there are many difficulties; a number of which are still unresolved. The most important one is the mesh dependency of the finite element analysis, in which by continually refining the mesh, we can make the crack propagate at lower and lower loads[12].

One model that provides a simple approach to localization zone simulation is the Rankine softening plasticity model and in this work a bilinear local softening model is adopted [13]. The position of the stress point on the softening branch, or the value of the fracture indicator, could be used as a measure, being compared to a predefined maximum value, to quantify the level of material damage for different regions.

In contrast to simple failure criteria, the interactive Tsai-Wu or Hoffman criteria do not provide any information regarding the crack direction. Therefore, a crack direction algorithm should be used to determine material crack directions once the failure criterion is satisfied. A simple, though sufficiently accurate, method is based on the assumption that the material cracks are only formed along or perpendicular to the fibre direction.

Another method for determining the crack direction is the so called acoustic tensor method, which was initially established for wave propagation problem in solids. In this method, it is proved that the discontinuity plane satisfies the acoustic tensor equation,

$$det\boldsymbol{A} = det\left(\boldsymbol{n} \cdot \boldsymbol{D}_{ct} \cdot \boldsymbol{n}\right) = 0 \tag{33}$$

where $\boldsymbol{A}$ is often referred to as the acoustic or characteristic tensor, $\boldsymbol{D}_{ct}$ is the elastoplastic consistent tangent matrix defined by (32), and the orientation of the discontinuity plane is described by the normal $\boldsymbol{n}$. The closed form solution may only be derived for two dimensional problems and a simple iterative approach is required to solve equation (33) for $\boldsymbol{n}$.

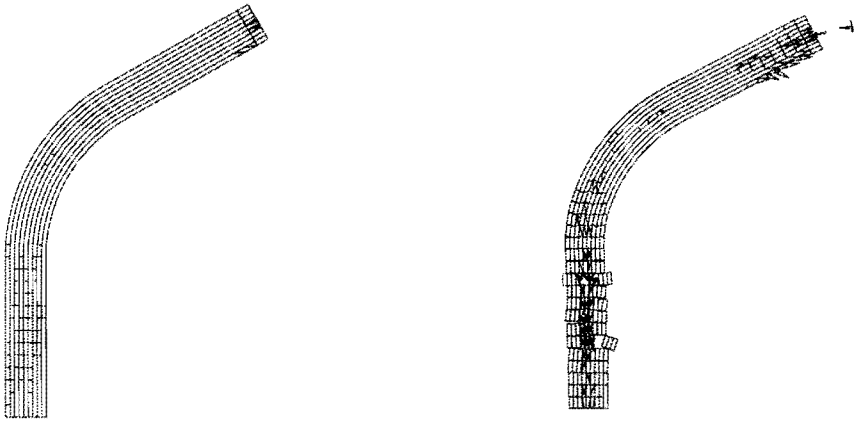

(a) Early fractures.

(b) Threshold of collapse

Figure 3: Fracture patterns of a 120-degree bend subjected to inward loading.

5 Numerical Results

5.1 Fracture Analysis of a Composite Bend

A 120-degree $[0_n, 90_n, 0_n]$ composite bend subjected to downward concentrated loading on its top end is considered. Each laminate is composed of Fiberite T300/1034-C graphite epoxy unidirectional tape (Table 1). Figure 3 represents the fracture patterns for two different stage of the loading. It is clearly observed that a progressive fragmentation process is localized within the weak mid layer around the supporting base of the bend.

Table 1: Material properties for T300/1034-C graphite epoxy.

$E_{xx} = 146800MPa$	,	$G_{xx} = 6184MPa$
$E_{yy} = 11400MPa$	,	$G_{yz} = 4380MPa$
$\nu_{xy} = \nu_{yz} = 0.3$	,	$\rho = 1.55\frac{Mg}{m^3}$
$X_t = 1730MPa$	,	$X_c = 1380MPa$
$Y_t = 66.5MPa$	,	$Y_c = 26.8MPa$
$S = 133.7MPa$		

5.2 Impact Loading of a Composite Plate

A numerical simulation is undertaken to assess the performance of the method for dealing with progressive fracture and debonding phenomena in a laminated composite plate which is subjected to a high velocity impact at its centre. The impact loading is simulated by a triangular load applied from 0 to 5 μsec with a peak force of 1 kN. Because of symmetry, only one quarter of plate is modelled. Also, only the central region of this model is meshed by a DE mesh (See Figure 4a). Material properties and other necessary information are given in Figure 4b) [14].

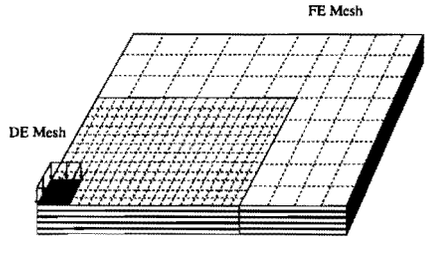

Model size $= 0.0762 \times 0.0508 \times 0.00444m$		
DE region $= 0.050 \times 0.035m$		
Ply layout $[90, 0, 90, 0, 90]$		
$E_{xx} = 152.4e3MPa$	,	$E_{yy} = 10.7e3MPa$
$\nu = 0.35$	,	$\rho = 1.55e3\frac{Kg}{m^3}$
$X_t = 2772MPa$	,	$X_c = 3100.0MPa$
$Y_t = 79.3MPa$	,	$Y_c = 231.0MPa$
$S = 132.8MPa$		

Figure 4: FE/DE mesh of the composite plate.

Vertical displacement responses of individual layers are shown in Figure 5. The clear discontinuities of the contours in certain parts of the model near the loading region mark the material fracture patterns. Matrix cracking has caused the cracks to be formed along the fibre direction in each layer.

6 CONCLUSIONS

An anisotropic softening Hoffman failure criterion is adopted within a combined finite/discrete element method, which has proved to be an efficient algorithm for dealing with multi-fracture and fragmentation processes. In addition to considering the potential pre-delamination contacts, it is also essential to take into account the contact and friction interactions for post

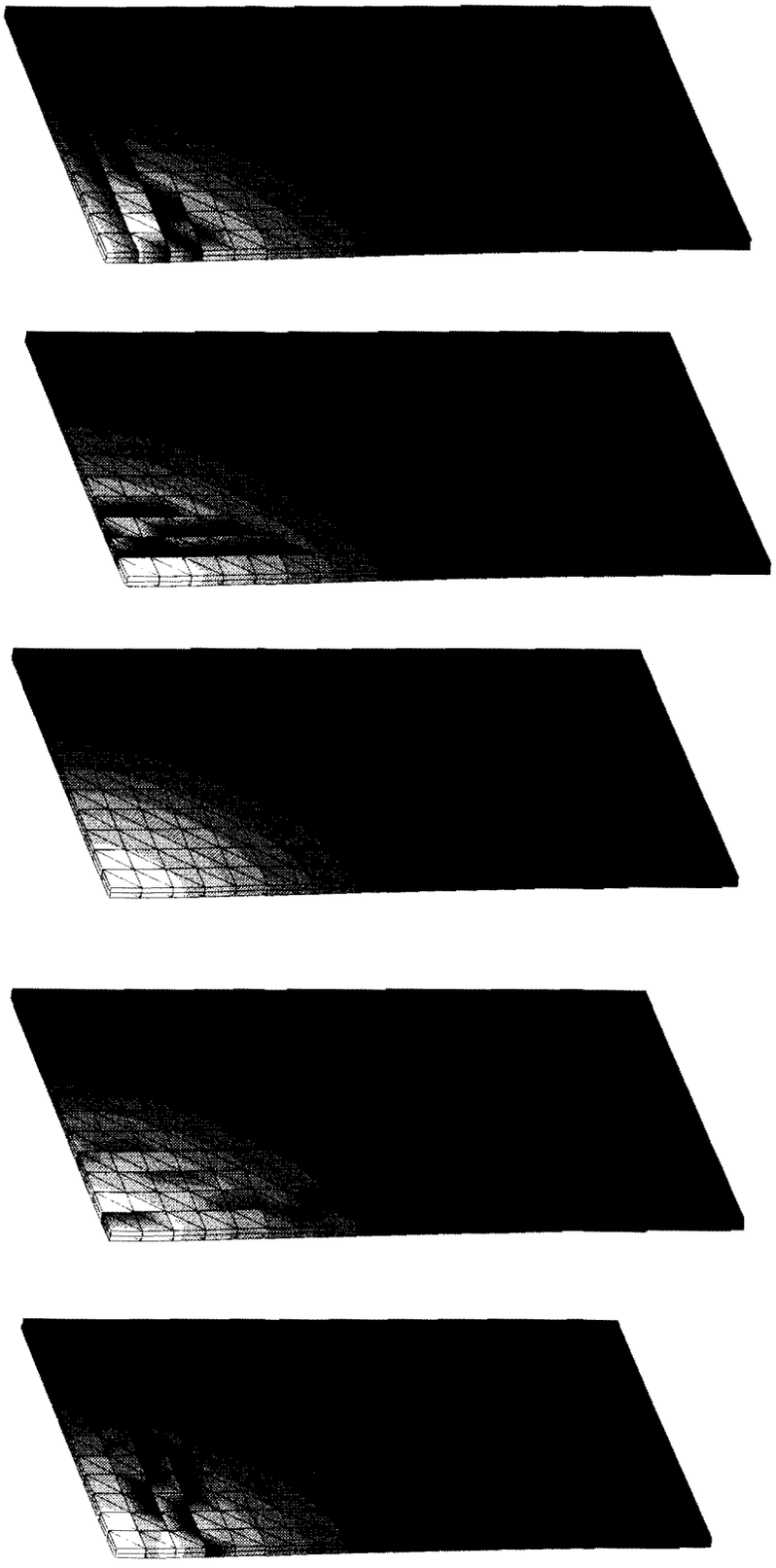

Figure 5: Vertical displacement and fracture patterns of different layers.

debonding or fracture behaviour of composites. A major advantage of the method is that it does not require any predefined interface elements, which are considered inappropriate for efficient computational modelling of combined progressive multi-fracture and delamination analysis.

7 Acknowledgements

The author would like to gratefully appreciate his colleagues Prof. D.R.J. Owen and Dr. D. Peric who were closely involved in the developing stage of the work, and the Rockfield Software Ltd. for providing the software support. The author would also like to acknowledge the support received from the Ministry of Higher Education of I.R. IRAN.

References

[1] C.G. Koh, D.R.J. Owen, and D. Peric. Explicit dynamic analysis of elasto-plastic laminated composite shells: implementation of non-iterative stress update schemes for the hoffman yield criterion. *Computational Mechanics*, **16**:307–314, 1995.

[2] F.L. Matthews and R.D. Rawlings. *Composite Materials : Engineering and Science.* Chapman and Hall, 1994.

[3] S. Mohammadi, D.R.J. Owen, and D. Peric. Delamination analysis of composites by discrete element method. In D.R.J. Owen, E. Onate, and E. Hinton, editors, *Computational Plasticity, COMPLAS V*, pages 1100–1110, March 1997. Barcelona, Spain.

[4] Y. Mi, M.A. Crisfield, and G.A.O. Davies. Failure modelling in composite structures. In M.A. Crisfield, editor, *Computational Mechanics in UK - 5th ACME Conference*, pages 36–39, April 1997. London, UK.

[5] S. Mohammadi, D.R.J. Owen, and D. Peric. A combined finite/discrete element algorithm for delamination analysis of composites. *Finite Elements in Analysis and Design*, **28**:321–336, 1998.

[6] R.E. Rowlands. Strength (failure) theories and their experimental correlation. In G.C. Sih and A.M. Skudra, editors, *Handbook of Composites, Vol. 3 - Failure Mechanics of Composites*, chapter 2, pages 71–125. Elsevier Science Publishers B.V., 1985.

[7] E.Z. Stowell and T.S. Liu. On the mexhanical behaviour of fiber-reinforced crystalline materials. *Journal of Mechanical Physics of Solids*, **9**:242–260, 1961.

[8] O. Hoffman. The brittle strength of orthotropic materials. *Journal of Composite Materials*, **1**:200–206, 1967.

[9] S.W.Tsai and E.M.Wu. A general theory of strength for anisotropic materials. *Composite Materials*, **5**, 1971.

[10] J.K. Simo and R.L. Taylor. A return mapping algorithm for plane stress elastoplasticity. *International Journal of Numerical Methods in Engineering*, **22**:649–670, 1986.

[11] C.J. Pearce. *Computational Plasticity in Concrete Failure Mechanics.* PhD thesis, Department of Civil Engineering, University of Wales Swansea, 1996.

[12] M.A. Crisfield. *Non-linear Finite Element Analysis of Solids and Structures. Volume 2: Advanced Topics.* John Wiley & Sons Ltd., 1997.

[13] A. Munjiza, D.R.J. Owen, and N. Bicanic. A combined finite-discrete element method in transient dynamics of fracturing solids. *Engineering Computations*, **12**:145–174, 1995.

[14] M.J. Worswick, P.V. Strazincky, and O. Majeed. Dynamic fracture of fiber reinforced composite coupons. In C.T.Sun, B.V. Sankar, and Y.D.S. Rajapakse, editors, *Dynamic Response and Behaviour of Composites*, ASME AD-Vol. 46, pages 29–41, 1995.